Design of New Concept Permanent Magnet Induction Wind Generator

Johannes H.J. Potgieter and Maarten J. Kamper, *Senior Member, IEEE*
Department of Electrical and Electronic Engineering
University of Stellenbosch
Private Bag X1, Matieland, 7602, South Africa
kamper@sun.ac.za

Abstract—**The construction and design of a new concept permanent magnet induction wind generator for direct grid-connection is proposed and evaluated in this paper. The use of non-overlap windings in this type of generator is proposed for the first time and analysed. Combined analytical and finite element calculation and design-optimisation methods are developed and used in the design of the generator. The cogging ripple torque is very important and is minimised to an absolute minimum in the design optimisation. An overall efficiency of higher than 92 % over a wide load range is obtained of a 15 kW permanent magnet induction wind generator.**

Keywords – Design, permanent magnet, induction, wind generator, finite element.

I. INTRODUCTION

The permanent magnet induction generator (PMIG) makes use of an additional free rotating PM rotor between the stator and rotor of an induction machine or in the inside of the rotor (or outside of the stator) as shown in Fig. 1a. The PM rotor supplies the magnetic flux within the machine and induces a voltage in the stator winding as shown in the equivalent circuit of Fig. 1b. This, in principle, reduces the magnetizing current and improves the power factor of the machine. The idea originated from [1] in 1926, followed by [2] and [3] using PM material. In 1992, [4] uses high energy product PMs for the first time. The design of the PMIG for large (2 MW) wind turbines was investigated by [5 – 7]. Other research was done in Japan [8], [9] and recently a proposal was investigated for the use of PMIGs in solid state converter (SSC) fed wind farms with HVDC transmission [10]. The application is clearly for generators in renewable energy systems.

In all the literature, hitherto, the design and modelling of this type of generator are based on the conventional PMIG layout as in Fig. 1, using standard stator and cage rotor windings. Experimental testing was done on only low pole number machines. Nothing has been reported in literature about the cogging effect between the PM rotor and the stator or rotor; cogging causes the PM rotor to lock with the stator and rotor teeth. Furthermore, transient *dq*-axis modeling of this type of generator is lacking in literature.

The advantages of PMIGs for wind generator applications are very attractive as they avoid the use of gearboxes and the use of power electronic converters for grid-connection. The device is, thus, a direct-drive direct-grid energy converter which is a very attractive concept. But in spite of these advantages and all the research done, up to now not a single PMIG wind generator has been installed and tested in practice as far as the authors know. The main reasons for this is probably the difficult construction and the fixed speed operation. The fixed-speed disadvantage of the PMIG is not a disadvantage with HVDC transmission. With HVDC transmission all the PMIGs in the wind farm are connected to the same grid of which the grid frequency is controlled via the converter according to the wind speed. In this way, thus, maximum power point tracking is possible. This is probably one of the most attractive features of PMIGs. But even with fixed grid frequency operation it is debatable if this is a disadvantage. What is important is the annual energy production per cost of the system; the energy production of fixed-speed PMIG wind turbines is lower, but the cost is also predicted lower with no gearboxes and SSCs.

With regard to efficiency there is also no disadvantage. The PMIG can be considered as two machines in tandem, multiplying, thus, two efficiencies. But a normal PM direct-drive generator with an SSC also has two converter actions in tandem and so does the double-fed induction generator plus gearbox system.

In this paper a new approach is followed in the construction and the design of a PMIG for wind generator applications. The practical tests are done at a 15 kW power level.

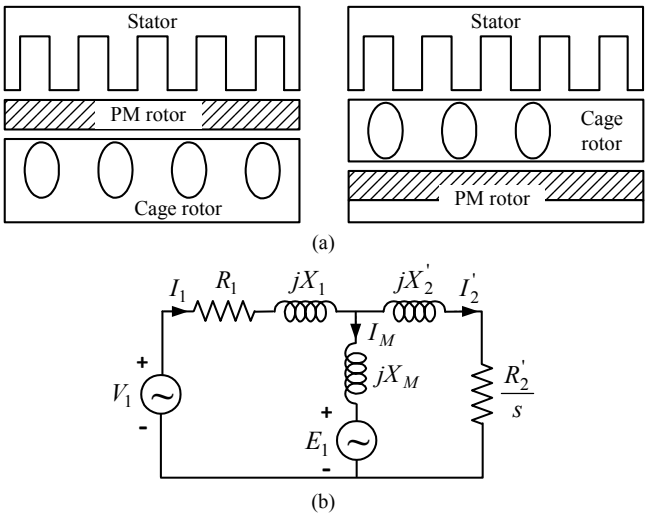

Fig. 1. (a) Cross-section and (b) equivalent circuit of conventional PMIG.

II. NEW CONCEPT PMIG

A new concept of the PMIG not reported in literature is to magnetically split the PMIG into two PM generators linked by a freely rotating PM rotor. The one generator is a synchronous generator (SG) with its stationary stator connected to the grid. The other generator operates as an induction generator (IG) with its short-circuited rotor mechanically connected to the turbine, which runs at slip speed with respect to the synchronously rotating PM rotor.

The magnetically split PMIG can thus be modelled as two separate, decoupled machines as shown in the per phase equivalent circuit of Fig. 2a. The per phase induced voltages in both machines are due to the rotating PM rotor; in the case of the synchronous machine a voltage is induced in the stator at grid frequency and in the case of the induction machine a voltage is induced in the induction rotor at slip frequency. Note that the rotor circuit in Fig. 2a is referred to grid frequency, and slip and slip speed is taken as positive in generator mode. Power transfer, thus, takes place from the turbine to the induction rotor and then via the PM rotor to the stator and the grid.

Comments on the split PMIG (S-PMIG) versus the coupled PMIG (C-PMIG) of Fig. 1a are the following: (i) the amount of PM material used in the S-PMIG is the same as in the C-PMIG; (ii) the yoke-mass of the S-PMIG will be higher, but this will be low in high pole number machines relative to the total mass; (iii) the number of poles and size of the IG and the SG in a S-PMIG can differ, which is advantageous from a design point of view; this is not possible in a C-PMIG; (iv) with a S-PMIG, non-overlap windings can be used in both the SG and IG, which is a huge advantage in terms of reduced cogging and load torque ripple and a lower number of coils; a low cogging torque cannot be overemphasized as it affects the start-up of the PMIG and the stability of the freely rotating PM rotor, specifically at low slip speeds; (v) in a S-PMIG with the IG and SG mounted in tandem as shown in Fig. 2b, the air gap diameters of both the IG and SG can be put to a maximum to maximise generated torque.

The mechanical construction of a small (15 kW) S-PMIG wind generator proposed and investigated in this paper is shown in Fig. 2b. The IG's PM-rotor is fixed to the SG's PM-rotor, while the IG's non-overlap rotor bar winding and core is mounted onto the turbine mounting plate; in the case of a single layer non-overlap rotor bar winding, the short-circuited single turn rotor bar coils can be manufactured separately and then inserted into the rotor slots. Furthermore, the IG part of the generator can be completely removed and the turbine can be mounted directly on the SG's mounting plate, resulting then in a normal PM wind generator connected to the grid via an SSC.

It can be seen from the drawing in Fig. 2b that the axial stack length of the IG-rotor is shorter than that of the SG-stator, with both at the same power rating. This is due to the much better conductor filling factor of the rotor bar winding. Furthermore, an extra set of bearings is used in the PMIG, which normally receive negative comments. The extra set of bearings, however, operates only at slip speed, and are also far fewer than the number of bearings used in a gearbox system.

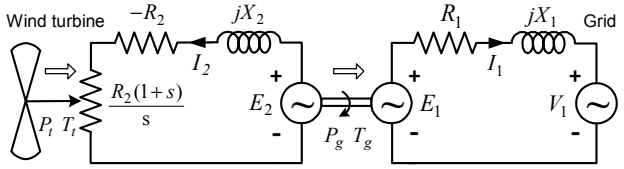

(a)

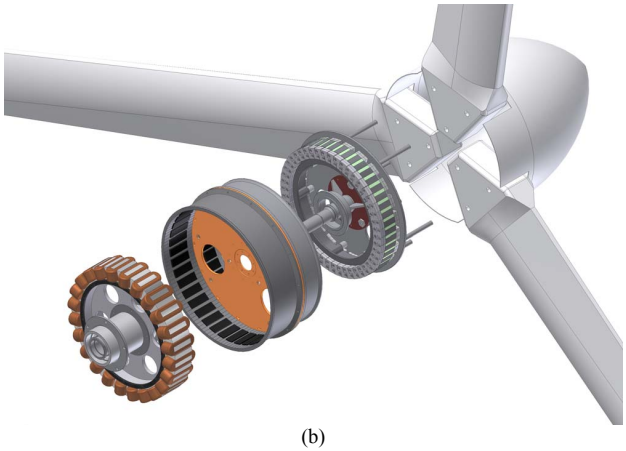

(b)

Fig. 2. Equivalent circuit and cross section of new split PMIG.

III. PMIG MODELLING

Both the design optimisation and the performance evaluation of the S-PMIG are done with the machine in the steady state and in the *dq* reference frame fixed to the rotor. The steady state *dq* equations of the IG and SG are given from Fig. 3 respectively by [positive current is taken as flowing out]

$$\begin{aligned} 0 &= -R_r I_{qr} - \omega_{sl} L_{dr} I_{dr} + \omega_{sl} \lambda_{mr} \\ 0 &= -R_r I_{dr} + \omega_{sl} L_{qr} I_{qr} \end{aligned} \tag{1}$$

and

$$\begin{aligned} V_{qs} &= -R_s I_{qs} - \omega_s L_{ds} I_{ds} + \omega_s \lambda_{ms} \\ V_{ds} &= -R_s I_{ds} + \omega_s L_{qs} I_{qs} , \end{aligned} \tag{2}$$

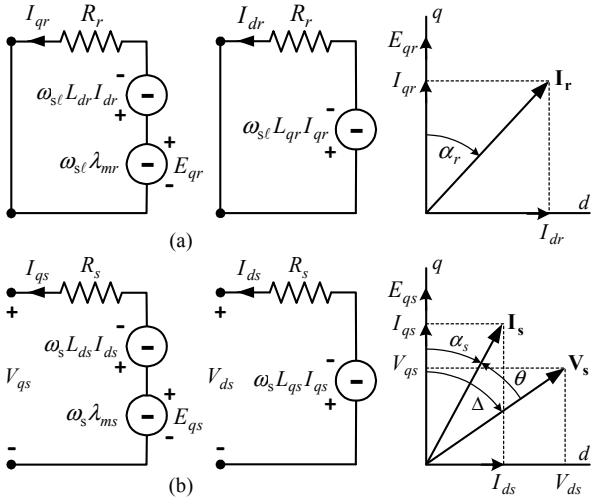

Fig. 3. Steady-state *dq* equivalent circuits and vector diagrams of (a) the IG and (b) the SG.

where ω_{sl} is the electrical slip speed equal to $\omega_{sl} = \omega_t - \omega_s$ with ω_t the electrical turbine speed and $\omega_s = 2\pi f$ the synchronous electrical speed, and where subscript "*r*" donates IG-rotor and "*s*" donates SG-stator. The load angle Δ, the current angle α and the SG's power factor angle $\theta = \Delta - \alpha_s$ are all defined in the vector diagrams of Fig. 3. The general relations of voltage, current and copper losses are given by (3) – (6) as

$$\begin{bmatrix} V_{qs} \\ V_{ds} \end{bmatrix} = \sqrt{2}\, V_{rms} \begin{bmatrix} \cos\Delta \\ \sin\Delta \end{bmatrix}; \quad \begin{bmatrix} I_q \\ I_d \end{bmatrix} = \sqrt{2}\, I_{rms} \begin{bmatrix} \cos\alpha \\ \sin\alpha \end{bmatrix}. \tag{3}$$

$$V_{qs}^2 + V_{ds}^2 = 2V_{rms}^2 \quad [V_{rms} = V_{grid}]; \tag{4}$$

$$I_q^2 + I_d^2 = 2I_{rms}^2 \tag{5}$$

and

$$I_{rms}^2 = \frac{P_{cu}}{3R}. \tag{6}$$

P_{cu} in (6) is the copper loss of the rotor or stator winding. The developed torque of both the IG and SG is given by

$$T_g = \frac{3}{4} p[(L_q - L_d) I_d I_q + \lambda_m I_q], \tag{7}$$

where the *dq* inductances are defined as

$$L_q = \frac{\lambda_q}{-I_q}; \quad L_d = \frac{\lambda_d - \lambda_m}{-I_d}. \tag{8}$$

The efficiency of the PMIG is given by

$$\eta = \eta_{IG}\, \eta_{SG}\ , \tag{9}$$

where

$$\eta_{IG} = \frac{P_{gr}}{P_t} = \frac{T_{gr}\omega_{sm}}{T_{gr}\omega_{tm}} \tag{10}$$

and

$$\eta_{SG} = \frac{P_{gs}}{P_{gr}} = \frac{T_{gr}\omega_{sm} - (P_{ecs} + P_{wfs}) - P_{cus}}{T_{gr}\omega_{sm}} \tag{11}$$

and where subscript "*m*" donates mechanical speed. In (11), P_{wfs} and P_{ecs} are respectively the wind-and-friction and the eddy-current-and-core losses of the SG. Note that P_{wfr} and P_{ecr} of the IG are practically zero, thus from (10) the only remaining (copper) losses are given by $P_{cur} = T_{gr}\omega_{s\ell m}$. The torque of the SG is also given from (11) by

$$T_{gs} = T_{gr} - \frac{(P_{ecs} + P_{wfs})}{\omega_{sm}}. \tag{12}$$

P_{ecs} in (11) and (12) includes the eddy current losses in the magnets and PM yoke of the SG, which can be substantial when using solid magnets and solid rotor yokes [11], [12]. With the generator operating at a constant speed, P_{wfs} is considered as constant in the modelling and is calculated once. The stator core losses of the SG are calculated by means of an empirical formula using, amongst other things, the air gap flux density data from FE analysis. The SG's eddy current losses in the magnets and PM yoke are also determined once [after the design optimisation] from FE transient loss calculations.

Finally, the SG's working power and reactive power supplying to or consuming from the grid are given by

$$\begin{bmatrix} P_{gs} \\ Q_{gs} \end{bmatrix} = 3V_{rms} I_{rms} \begin{bmatrix} \cos\theta \\ \sin\theta^* \end{bmatrix}. \tag{13}$$

The cross-sections and FE modelling of the non-overlap winding PMIG and PMSG are shown in Fig. 4. As the grid frequency is 50 Hz and the rated turbine speed is 150 r/min, the number of poles for the SG is p = 40; the same number of poles is also used for the IG in this case. With p = 40 and choosing the high winding factor 10-12 pole-slot combination, five poles and six slots form a machine section in the FE model using negative periodic boundary conditions. For both the IG and SG surface-mounted PMs are used. For the IG, both single and double layer rotor bar windings are investigated, but for the SG only a single layer winding with preformed coils is considered. In the case of the IG, solid rotor yokes are used as the eddy current frequencies are very low. In the case of the SG both laminated and solid partial-segmented rotor yokes are considered as investigated in [11].

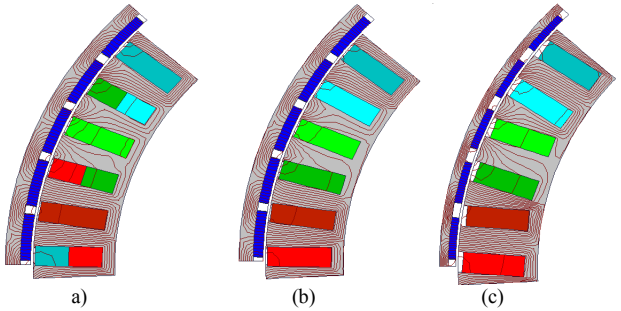

a) (b) (c)

Fig. 4. Cross section and FE plot of (a) double layer IG, (b) single layer IG and (c) single layer SG.

IV. Design Optimisation

The optimum design of only the PM rotor and rotor winding of the IG shown in Fig. 4a and b are considered in this paper. The design of the SG is thoroughly covered in [13]. The design optimisation of the 15 kW IG is done subject to the required performance of the machine given by $\mathbf{U_{IG}}$ and $\mathbf{G_{IG}}$ as

$$\mathbf{U_{IG}} = \begin{bmatrix} P_{gr} \\ \omega_{sm} \\ \eta_{IG} \end{bmatrix} = \begin{bmatrix} 15.96\ \text{kW} \\ 15.71\ \text{rad/s} \\ 98.3\ \% \end{bmatrix} \Rightarrow \mathbf{G_{IG}} = \begin{bmatrix} T_{gr} \\ P_{cur} \\ \omega_{s\ell m} \end{bmatrix} = \begin{bmatrix} 1016\ \text{Nm} \\ 276\ \text{W} \\ 0.27\ \text{rad/s} \end{bmatrix} \tag{14}$$

where P_{gr} = 15 kW/η_{SG} with η_{SG} = 94 % given, and where the synchronous speed is 150 r/min. The IG's efficiency is taken very high in (15) to ensure an overall efficiency of η > 92 %. Note from (14) that the rated slip is 1.73 %, and that a lower required efficiency will increase the rated slip.

The design optimisation of the IG is done by maximising the torque per copper losses of the machine. Maximising the torque per copper losses at a fixed speed is the same as maximising the efficiency of the IG as the core losses of the IG are practically zero. The objective function to be maximised in the optimisation, thus, is given by

$$\mathbf{F(X)} = \frac{T_{gr}}{P_{cur}}(\mathbf{X}), \tag{15}$$

where **X** is a dimensional vector that includes all the dimensions of the machine to be optimised. These dimensions include the magnet pitch, slot pitch (in the case of the single layer winding), slot opening, slot width, yoke heights, magnet height and air gap diameter of the IG. The outer and inner stack diameters are the same as that of the SG and are kept constant in the optimisation. After the design optimisation the axial stack length of the IG is adjusted so as to obtain the required performance of (14) at rated copper losses. At this new axial length a next design optimisation is executed to confirm the optimum design.

The design optimisation is done by means of an optimisation algorithm (Powell's algorithm [14]) that is integrated with the FE program. With each iteration the optimisation algorithm calls the FE-program to calculate the function value of (15) for a given **X**. The FE-program then re-meshes the machine structure according to **X** and calculates the function value by means of a number of non-linear static FE solutions. This is done as follows:

(i) I_{rms} is calculated from (6), at the rated copper losses of (14) and with R_r calculated analytically according to the given slot dimensions.

(ii) With I_{rms} known and $\alpha_r = 0$, λ_{mr} is first calculated from one FE solution, i.e. by transforming the FE-calculated phase flux linkages to *dq* parameters using Park's transformation. In this way the effect of the q-axis current, I_{qr}, on λ_{mr} is taken into account.

(iii) With I_{rms} known, and at a relatively small, chosen current angle α_r, initial values for I_{dr} and I_{qr} are calculated.

(iv) With currents and current angle known, a FE solution is used to calculate λ_{dr} and λ_{qr}, and, hence, L_{dr} and L_{qr} according to (8).

(v) With λ_{mr}, I_{rms} and initial values for L_{dr} and L_{qr} known, new values for I_{dr} and I_{qr} and the slip speed $\omega_{s\ell}$ are calculated by solving simultaneously from (1) and (5).

(vi) With new I_{dr}, I_{qr} currents and a new current angle α_r, steps (iv) and (v) are repeated for higher accuracy in the calculation of the *dq* currents; if found necessary another iteration can be executed.

(vii) With currents and inductances known, T_{gr} of (7) and **F(X)** of (15) are finally calculated and returned to the optimisation algorithm. A total number, thus, of say three to four static FE solutions are used to calculate the function value.

After completion of the optimum design as described above, the cogging torque of the IG is next minimised by further adjustments of the magnet pitch and the slot opening of the IG; these dimensions have the largest effect on the cogging torque. A sensitivity analysis procedure is followed to determine the sensitivity of the cogging torque to magnet pitch and slot opening variations. These results are shown in Fig. 5a and are obtained from a high number of static FE solutions. It is clear from Fig. 5a and b that there are regions where the cogging torque is fairly independent of dimensional change and where the cogging torque is very low (less than 1 %). Also shown in Fig. 5c is the relatively low sensitivity of the generated torque to magnet pitch variation, fairly independent of slot opening.

The final machine dimensions found from the design optimisation and the cogging torque minimisation are given in Table I; the optimum cross section layouts of the IG are shown in Fig. 4a and b. Also given in Table I is the rated performance of the IG. At the relatively high efficiency of 98.3 % the active mass of the optimum designed IG is 70 % that of the optimum designed SG, mainly due to the much better filling factor using rotor bars.

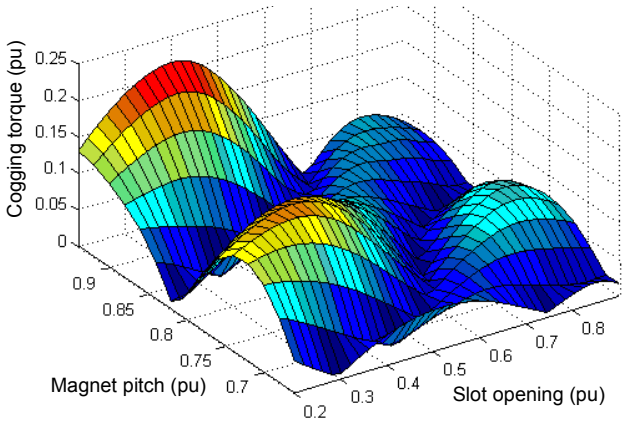

(a)

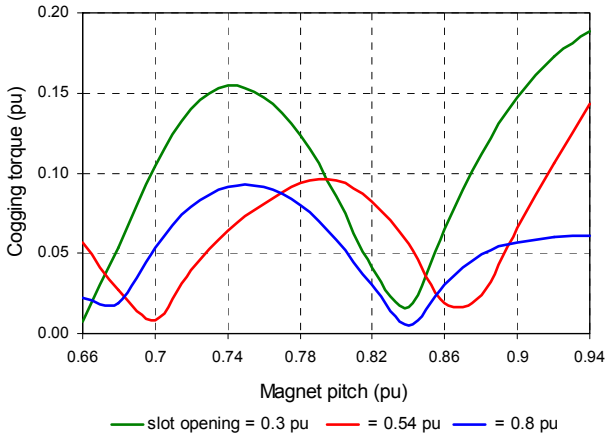

(b)

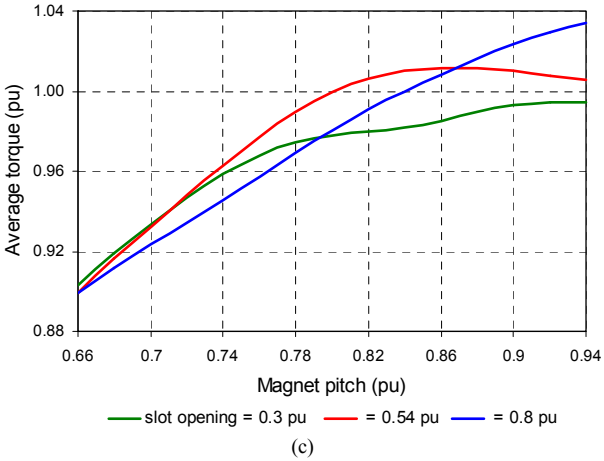

(c)

Fig. 5. Sensitivity of cogging torque and average torque to magnet pitch variation and slot opening a parameter of the IG, with P_{cur} constant. (values: 1 pu magnet pitch = pole pitch; 1 pu slot opening = slot width)

TABLE I.
DIMENSIONS AND PERFORMANCE OF PMIG AT 50 Hz and 150 r/min.

Parameter	IG	SG
Outer diameter (mm)	652	653.5
Inner diameter (mm)	483	494
Magnet pitch / pole pitch	0.84	0.73
Air gap (mm)	2	2
Slot width (mm) [= 1 pu]	17.5	18
Magnet height (mm)	8	6
Yoke height (mm)	10	10
Magnet-yoke height (mm)	11.5	7.25
Axial length (mm)	62.5	100
Torque (Nm)	1000	1000
Efficiency (%)	98.3	94.4
Rated slip (%)	1.76	-
L_d/L_q at rated load	1.5	1.4

V. SIMULATION METHOD

As the PMIG wind generator system is an uncontrolled system as shown in Fig. 2a, the currents of (1) and (2) have to be solved in order to simulate the steady state performance of the PMIG versus load, i.e. versus slip speed.

For quick simulation results the *dq* inductances of both the IG and SG are first determined as functions of current. This is done by calculating λ_m at no-load and *dq* flux linkages at load from static FE solutions, and then using (8). The *dq* inductances calculated in this way of e.g. the IG are shown in Fig. 6. This shows the drastic effect of saturation and cross-magnetisation on the *dq* inductances of (even) a surface-mounted PM machine.

For the simulation of the IG's performance versus load the slip frequency $\omega_{s\ell} = \omega_t - \omega_s$ of (1) is taken as a given input parameter. I_{dr} and I_{qr} are then determined by solving (1) simultaneously, using initial values for L_{dr} and L_{qr} obtained from Fig. 6. With new values for I_{dr} and I_{qr}, L_{dr} and L_{qr} are updated in a second iteration from Fig. 6, followed by calculating I_{dr} and I_{qr} by solving (1) again. For higher accuracy further iterations may be followed. With I_{dr} and I_{qr} and L_{dr} and L_{qr} known, the torque and the efficiency of the IG for the given slip speed can be determined from (7) and (10).

In exactly the same way as the IG the SG's *dq* currents I_{ds} and I_{qs} are determined by solving (2) simultaneously. In this case V_{rms} and ω_s are known, and Δ is the variable input parameter; V_{ds} and V_{qs} are, thus, known from (3). At each slip speed and calculated IG's torque, Δ is increased iteratively to increase the SG's torque until the required torque of (12) is obtained. At this Δ the power and reactive power of the SG are calculated from (13).

VI. PERFORMANCE RESULTS

Some of the performance results of the simulations and measurements are shown in Figs. 7 – 11. Almost a close to zero percentage cogging torque is obtained as shown in Fig. 7. Fig. 8 shows the torque performance versus slip of the IG and SG short-circuited; the IG develops rated torque at just less than 2 % slip and has a pull-out torque of 2.0 per unit. Excellent overall efficiency of higher than 92 % is obtained for a wide torque range as shown in Fig 9. Also the measured efficiency of the SG compares very well with the calculated results. The variation of the reactive power with load as shown in Fig. 10, with grid voltage a parameter, is very interesting – it implies that the generator can be designed to supply at low loads capacitive reactive power to the grid, but at high loads to draw reactive power, which is exactly how grid voltage compensation is done. Otherwise, if reactive power flow is undesirable, use can be made of tap-changing transformers. Figure 11 shows the leading current of the SG under low grid voltage conditions measured in the laboratory.

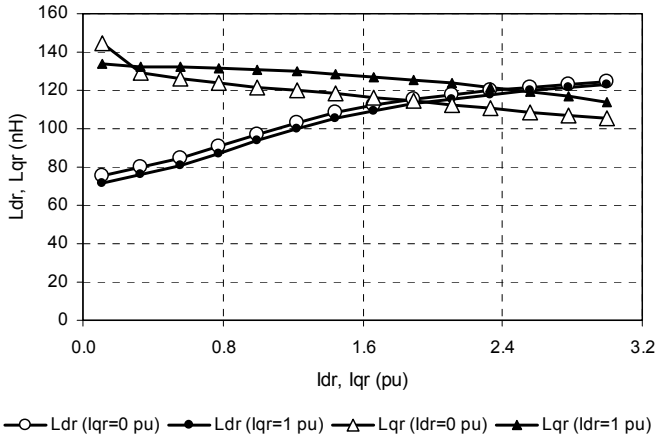

Fig. 6. *dq* inductances versus *dq* current of the IG.

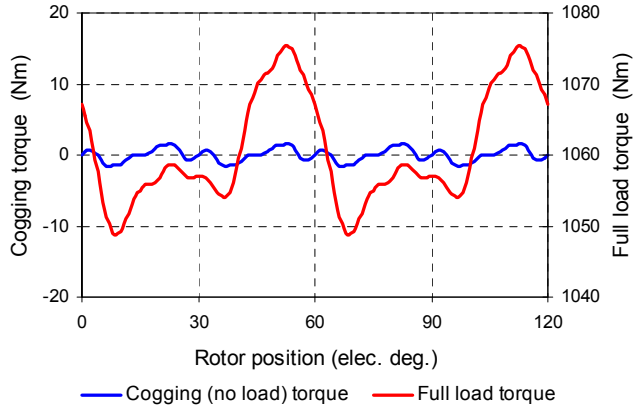

Fig. 7. Cogging and load torque of the IG.

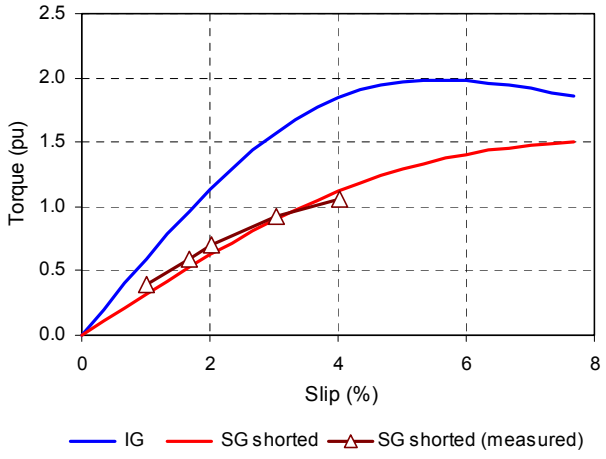

Fig. 8. Torque versus slip of the IG and shorted SG.

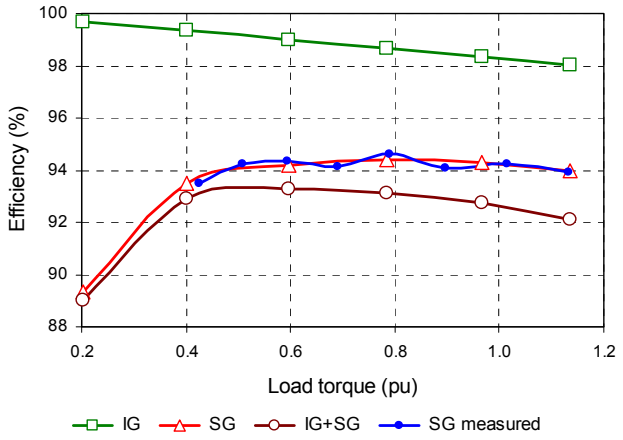

Fig. 9. Efficiency versus load of the 15 kW PMIG.

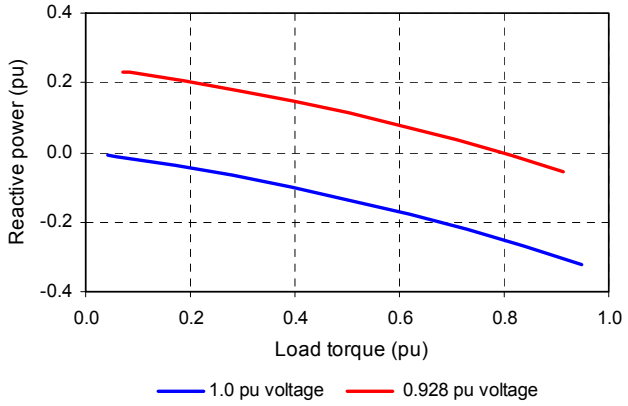

Fig. 10. Reactive power flow versus load of the 15 kW PMIG.

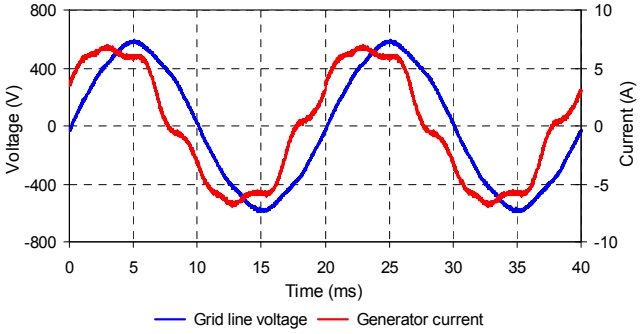

Fig. 11. Measured voltage and current of the grid-connected SG at almost no-load and 0.926 pu grid voltage (433 V = 1 pu voltage).

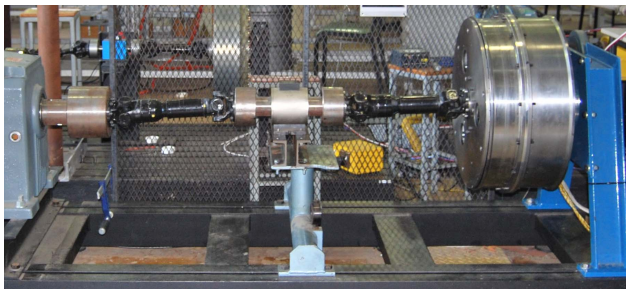

Fig. 12. 15 kW PMIG wind generator (right) under test via a torque sensor (middle) and drive system (left).

VII. Conclusions

The new proposed split PMIG with non-overlap windings for both the IG and SG is shown to give good results in terms efficiency over a wide load range. Saturation and cross magnetisation have a significant effect on the *dq* inductances and the developed torque of the surface mounted PM IG and SG. The relatively high measured cogging torque of 4.5 % of the IG is attributed to magnet and manufacturing inequalities. With the non-overlap rotor bar winding the rated torque of the IG is obtained at a fairly low slip frequency of just less than 2 %; a pull-out torque of 2.0 per unit is predicted with this type of winding. It is shown that the PMIG compensates automatically for grid voltage variation. For the prototype PMIG the SG comprises about 60 % of the total mass of the generator and the IG (with copper rotor bars) about 40 % of the mass. This mass ratio, however, can be improved by using e.g. aluminum IG rotor bars.

References

[1] F. Punga and L. Schon, "Der neue kollektorlose einphasenmotor der Firma Krupp", Elektro-technishe Zietschrift, Bucharest, Rumania, vol. 47, pt 1, no. 29, pp 842-847; pt II, pp 877-881, July 1926.

[2] J.F.H. Douglas, "Characteristics of induction motors with permanent magnet excitation", Trans. AIEE (PAS), vol. 78, pp 221-225, June 1959.

[3] J.K. Sedevy, "Induction motor with freely rotating d.c. excitation", Trans. AIEE (PAS), vol. 86, no. 4, pp 463-469, 1967.

[4] W.F. Low, N. Schofield, "Design of a permanent magnet excited induction generator", Proc. of the Int. Conf. on Electrical Machines (ICEM), Manchester (United Kingdom), 1992, vol. 3, pp. 1077-1081.

[5] B. Hagenkort, T. Hartkopf, A. Binder and S. Jockel, "Modelling a direct drive permanent magnet induction machine", Proc. of the Int. Conf. on Electrical Machines (ICEM), Espoo (Finland), Aug. 2000, pp. 1495-1499.

[6] G. Gail, Th. Hartkopf, E. Tröster, M. Hoffling, M. Henschel and H.Schneider, "Static and dynamic measurements of a permanent magnet induction generator: test results of a new wind generator concept", Proc. of the Int. Conf. on Electrical Machines (ICEM), Cracow (Poland), Sept. 2004.

[7] E. Tröster, M. Sperling and Th. Hartkopf, "Finite element analysis of a permanent magnet induction machine", Int. Symposium on Power Electronics, Electrical drives, Automation and Motion (SPEEDAM), 2006.

[8] T. Fukami, K. Nakagawa, Y. Kanamaru and T. Miyamoto, "A technique for the steady-state analysis of a grid-connected permanent magnet induction generator", IEEE Trans. on Energy Conversion, vol. 19, no. 2, pp 318-324, June 2004.

[9] T. Tsuda, T. Fukami, Y. Kanamaru and T. Miyamoto, "Effects of the built-in permanent magnet rotor on the equivalent circuit parameters of a permanent magnet induction generator", IEEE Trans. on Energy Conversion, vol. 22, no. 3, pp 798-799, Sept. 2007.

[10] R. Vermaak, J.H.J. Potgieter and M.J. Kamper, "Grid-Connected VSC-HVDC wind farm system and control using permanent magnet induction generators", IEEE International Conference on Power Electronics and Drive Systems (PEDS), Tapei, Taiwan, Nov. 2009.

[11] D.A. Wills and M.J. Kamper, "Reducing PM eddy current losses by partial magnet and rotor yoke segmentation", Proc. of the Int. Conf. on Electrical Machines (ICEM), Rome (Italy), Sept. 2010.

[12] D.A. Wills and M.J. Kamper, "Analytical prediction of rotor eddy current loss due to stator slotting in PM machines", IEEE Energy Conversion Congress and Expo (ECCE), Atlanta (USA), Sept. 2010.

[13] J.H.J Potgieter and M.J. Kamper, "Cogging torque sensitivity in design optimisation of low cost non-overlap winding PM wind generator", Proc. of the Int. Conf. on Electrical Machines (ICEM), Rome (Italy), Sept. 2010.

[14] M.J.D. Powell, "An efficient method for finding the minimum of a function of several variables without calculating derivatives", Computer Journal, vol. 7, pp. 155-162, 1964.